Box C/D snoRNPs: solid-state NMR fingerprint of an early-stage 50 kDa assembly intermediate

Marie-Eve Chagot[1], Marc Quinternet[2], Clémence Jacquemin[1,3], Xavier Manival[1,**], Carole Gardiennet[4,*]

1. IMoPA, UMR 7365 CNRS / Université de Lorraine, Campus Biologie Santé, Nancy, France
2. UMS-2008 IBSLor Université de Lorraine, CNRS, INSERM, Nancy, France
3. *Present address:* Centre International de Recherche en Infectiologie, Biologie Cellulaire des Infections Virales, INSERM, U1111, Université Claude Bernard Lyon 1, CNRS, UMR5308, École Normale Supérieure de Lyon, Hospices Civils de Lyon, Université de Lyon, Lyon, France
4. CRM2, UMR 7036 CNRS / Université de Lorraine, Faculté des Sciences et Technologies, Nancy, France

**: corresponding author, xavier.manival@univ-lorraine.fr
*: corresponding author, carole.gardiennet@univ-lorraine.fr

- Marie-Eve Chagot: ORCID: 0000-0001-6407-9131
- Marc Quinternet: ORCID: 0000-0002-8299-7136
- Xavier Manival: ORCID: 0000-0002-7717-7096
- Carole Gardiennet: ORCID: 0000-0002-4883-7403

Abstract

Many cellular functions rely on stable protein-only or protein-RNA complexes. Deciphering their assembly mechanism is a key question in cell biology. We here focus on box C/D small nucleolar ribonucleoproteins involved in ribosome biogenesis. The mature particles contain four core proteins and a guide RNA. Despite their relatively simple composition, these particles don't self-assemble in eukaryote and the production of a native and functional particle requires a large number of transient other proteins, called assembly factors. We present here ^{13}C and ^{15}N solid-state NMR assignment of yeast 126-residue core protein Snu13 in the context of its 50 kDa pre-complex with assembly factors Rsa1p[238-352]:Hit1p[70-164]. In this sample, only one third of the protein is labelled, leading to a low sensitivity. We could nevertheless obtain assignment data for 91% of the residues. Secondary structure derived from our assignments shows that Snu13p overall structure is maintained in the context of the complex. Chemical shift perturbations are analysed to evaluate Snu13p conformational changes and interaction interface upon binding to its partner proteins. While indirect perturbations are observed in the hydrophobic core, we find other good candidate residues belonging to the interaction interface. We describe the role of some Snu13p N-terminal and C-terminal residues, not identified in previous structural studies. These preliminary results will serve as a basis for future interaction studies, especially by adding RNA, to decipher box C/D snoRNP particles assembly pathway.

Keywords

solid-state NMR, *Saccharomyces cerevisiae*, box C/D snoRNP, Snu13p, protein-protein interaction

Acknowledgement

Financial support from PEPS Mirabelle 2016 "ssNMRsnoRNP" and from the IR-RMN-THC Fr3050 CNRS for conducting the research is gratefully acknowledged.

Biological context

Many cellular functions rely on stable protein-only or protein-RNA complexes. Deciphering their assembly mechanism is a key question in cell biology.
We here focus on specialized box C/D snoRNP particles (small nucleolar RiboNucleoProteins) that are in charge of a major post-transcriptional modification of the ribosomal RNA during ribosome biogenesis, the 2'-O-ribosome methylation. The mature eukaryotic box C/D snoRNP contains 4 core proteins, namely (mammal/yeast) SNU13/Snu13p, NOP58/Nop58p, NOP56/Nop56p and FIBRILLARIN/Nop1p and one snoRNA (Bachellerie et al., 2002). First, SNU13/Snu13p initiates the box C/D snoRNP assembly by interacting specifically with the k-turn motif of box C/D in snoRNA (Chagot et al., 2019; Watkins et al., 2002). The snoRNA:SNU13/Snu13p pre-snoRNP is required for the followed binding of NOP58/Nop58p and NOP56:Nop56p that assemble into a heterodimer (Schultz et al., 2006). The role of snoRNA is to guide, by base-pairing with rRNA sequence, the precise position of the nucleotide to modify. In addition, few others snoRNPs, including U3, U14 and U8 are required for endoribonucleolytic cleavages in the pre-rRNA (Lafontaine, 2015).
Despite their relatively simple composition, these snoRNP particles don't self-assemble in eukaryote (Peng et al., 2014) and the production of a native and functional particle requires a large number of transient other proteins, called assembly factors. We and others have contributed to the discovery of the box C/D snoRNP assembly machinery. In yeast, it includes in particular the Hsp90 co-chaperone complex R2TP composed of the AAA+ ATPases Rvb1 and Rvb2 and the proteins Tah1 and Pih1 (Boulon et al., 2008), the heterodimer Rsa1p:Hit1p (Rothé et al., 2014b), and the essential protein Bcd1 (Paul et al., 2019).

We use solid-state NMR (ssNMR) to get atomic-scale information on the early steps of *Saccharomyces cerevisiae* box C/D snoRNP assembly pathway, through the study of a protein complex composed of Snu13 core protein and domains of Rsa1p:Hit1p assembly factors. Snu13p shows 84% sequence identity with its human orthologue SNU13 (PDB 1E7K). Most of the interactions are transposable to human (Bizarro et al., 2014; Quinternet et al., 2016).

We report solid-state ^{13}C and ^{15}N assignments of the 126-residue core protein Snu13 in the context of the 50 kDa pre-complex Snu13p:Rsa1p[238-352]:Hit1p[70-164], named SRH in the following for the sake of simplicity. RH will refer to Rsa1p[238-352]:Hit1p[70-164].

Subsets of SRH complex have already been investigated, which provides useful data. Snu13p[4-125] X-ray diffraction structure has been solved (PDB 2ALE) (Dobbyn et al., 2007) and solution NMR chemical shifts of free Snu13p are available (Workman et al., 2008) (BMRB 15412). In these X-ray and NMR studies, free Snu13p bears respectively a C-terminal LG/LE+6H extension. Other structural data include X-ray structures of Snu13p[4-126]:Rsa1p[239-265] complex (PDB 4NUT) (Bizarro et al., 2014) and Rsa1p[317-352]:Hit1p[70-164] (PDB 2MJF) (Rothé et al., 2014b).

Our ssNMR SRH construct contains Rsa1p residues 260 to 316, not present in other available structural data and mostly predicted to be disordered (data not shown).

Materials and methods

Protein expression and purification; sample preparation

For the ssNMR sample, Snu13p and Rsa1p[238-352]:Hit1p[70-164] were produced in BL21(DE3) strain (NEB) containing the pRARE2 plasmid (Novagen) and transformed with the pnEA-3CH::Snu13p or co-transformed with pnEA-3CH::Rsa1[238-352] and pnCS::Hit1[70-164] (in-house vectors), in 2x1 L Luria Bertani medium for the unlabelled proteins, or M9 minimum medium supplemented with 0.5 $g.L^{-1}$ ^{15}N-NH_4Cl and 2 gL^{-1} ^{13}C-glucose (Cambridge Isotope Laboratories, Inc.). After overnight induction at 20°C with 0.2 mM IPTG when OD_{600} reaches 0.7, the cells were harvested at 8 000 rpm (Beckman Coulter Avanti JXN-26 centrifuge, JLA-8.1000 rotor) for 15 min at 10°C and the pellets resuspended in 30 mL of lysis buffer (HEPES-KOH 25 mM pH 7.5; NaCl 300 mM; imidazole 10 mM; TCEP 0.5 mM), sonicated and centrifuged at 20 000 rpm (Beckman Coulter Avanti J-20XP centrifuge, JA-20 rotor) for 30 min at 4°C. Supernatants were incubated with 0.0125% PEI for 15 min at 4°C to precipitate nucleic acids and centrifuged again at 20 000 rpm for 20 min at 4°C. Supernatants were filtered on a 0.45 µm filter and purified on affinity resin (Talon® Superflow Metal Affinity Resin, Clontech). The protein without the His6-tag was collected after overnight cleavage by PreScission protease on the beads.
After affinity purification, U-[^{13}C, ^{15}N] Snu13p and unlabelled Rsa1p[238-352]:Hit1p[70-164] were mixed, concentrated and purified on a gel filtration column (HiLoad® 16/600 Superdex® 200 pg , GE Healthcare) in HEPES-KOH 10mM pH 7.5; NaCl 150 mM; TCEP 0.5 mM; sodium azide 0.05%.
The elution peak corresponding to the reconstituted SRH complex was concentrated up to 50 mg/mL and ultracentrifuged overnight at 100 000 g at 4°C (SORVALL RC M120 GX centrifuge, S45A rotor). 15-20 mg sediment was transferred into a Bruker thin-wall 3.2 mm zirconium rotor (46 µL volume) by centrifugation thanks to a home-built filling device (Böckmann et al., 2009). SRH SDS-polyacrylamide gel is presented in the electronic supplementary material (**ESM figure 1**).

An additional sample of a sub-complex, U-[^{13}C, ^{15}N] Snu13p:Rsa1p[230-290], was prepared for solution NMR as described elsewhere (Rothé et al., 2014a).

NMR spectroscopy

SRH solid-state NMR spectra were recorded on 18.8 and 22.3 T Avance III Bruker spectrometers equipped with 3.2 mm E-free $^{1}H/^{13}C/^{15}N$ triple-resonance probes, at 278 K sample temperature, as determined by the resonance frequency of bulk water (Böckmann et al., 2009). Experimental details are given in **Table 1**.
Snu13p:Rsa1p[230-290] solution NMR spectra were acquired at 293 K on a 14.1 T Bruker Avance III spectrometer equipped with a TCI cryoprobe.

Chemical shifts were externally referenced to DSS (4,4-dimethyl-4-silapentane-1-sulfonic acid).

Table 1: solid-state NMR experimental parameters

Experiment	**DARR**	**DARR**	**DREAM**	**NCA**	**NCO**
external field (T)	18.8	22.3	22.3	18.8	18.8
MAS frequency (kHz)	17.5	18	18	17.5	17.5
Transfer 1	HC CP	HC CP	HC CP	HN CP	HN CP
Field (kHz)	66 (^{1}H) ; 50 (^{13}C)	68 (^{1}H) ; 50 (^{13}C)	61 (^{1}H) ; 45 (^{13}C)	57 (^{1}H) ; 41 (^{15}N)	57 (^{1}H) ; 41 (^{15}N)
Shape	tangent (^{1}H)	ramp (^{1}H)	ramp (^{1}H)	tangent (^{1}H)	tangent (^{1}H)
Carrier (ppm)	58 (^{13}C)	100 (^{13}C)	56 (^{13}C)	120 (^{15}N)	120 (^{15}N)
time (ms)	0.8	0.7	0.7	0.7	0.7
Transfer 2	DARR	DARR	DREAM	NC CP	NC CP
Field (kHz)	17.5 (^{1}H)	18 (^{1}H)	8 (^{13}C) ; 72 (^{1}H)	11.5 (^{15}N) ; 6 (^{13}C) ; 90 (^{1}H)	11.5 (^{15}N) ; 6 (^{13}C) ; 90 (^{1}H)
Shape	-	-	tangent (^{13}C)	tangent (^{13}C)	tangent (^{13}C)
^{13}C carrier (ppm)	100	100	56	58	177
time (ms)	20	50	2	4	4
t_1 increments	2812	952	1430	156	156
sw (t_1) (kHz)	93.75	59.501	59.524	9.725	9.725
Acq. Time (t_1) (ms)	15	7.99	12.01		8.02
t_2 increments	2802	1422	2374	1988	1988
sw (t_2) (kHz)	93.75	59.523	59.524	100	100
Acq. Time (t_2) (ms)	15	11.94	19.94	9.94	9.94
^{1}H decoupling	SPINAL-64	SPINAL-64	SPINAL-64	SPINAL-64	SPINAL-64
Field (kHz)	90	80	72	90	90
Interscan delay (s)	2	1.9	2.3	2	2
Number of scans	16	96	28	48	32
Measurement time (h)	24	48	22	4	2.75

Experiment	**NCACX**	**NCACX**	**NCACB**	**CANCO**
external field (T)	18.8	22.3	22.3	18.8
MAS frequency (kHz)	17.5	18	18	17.5
Transfer 1	HN CP	HN CP	HN CP	HC CP
Field (kHz)	57 (^{1}H) ; 41 (^{15}N)	67 (^{1}H) ; 40 (^{15}N)	61 (^{1}H) ; 45 (^{15}N)	66 (^{1}H) ; 50 (^{13}C)
Shape	tangent (^{1}H)	ramp (^{1}H)	ramp (^{1}H)	tangent (^{1}H)
Carrier (ppm)	120 (^{15}N)	120 (^{15}N)	120 (^{15}N)	58 (^{13}C)
time (ms)	0.7	0.9	0.9	0.8
Transfer 2	NC CP	NC CP	NC CP	CN CP
Field (kHz)	11.5 (^{15}N) ; 6 (^{13}C); 90 (^{1}H)	14 (^{15}N) ; 4 (^{13}C) ; 80 (^{1}H)	13.5 (^{15}N) ; 4 (^{13}C) ; 72 (^{1}H)	11.5 (^{15}N) ; 6 (^{13}C); 90 (^{1}H)
Shape	tangent (^{13}C)	tangent (^{13}C)	tangent (^{13}C)	tangent (^{13}C)
^{13}C carrier (ppm)	58	55	55	58
time (ms)	4	4	4	4
Transfer 3	DARR	DARR	DREAM	NC CP
Field (kHz)	17.5 (^{1}H)	18 (^{1}H)	8 (^{13}C) ; 72 (^{1}H)	11.5 (^{15}N) ; 6 (^{13}C); 90 (^{1}H)
Shape	-	-	tangent (^{13}C)	tangent (^{13}C)
^{13}C carrier (ppm)	100	100	55	177

time (ms)	80	60	2	4
t_1 increments	54	54	70	110
sw (t_1) (kHz)	3.242	3.851	4.333	8.044
Acq. Time (t_1) (ms)	8.33	7.01	8.08	6.84
t_2 increments	98	132	130	80
sw (t_2) (kHz)	7.039	9.558	9.558	5.573
Acq. Time (t_2) (ms)	6.96	6.9	6.8	7.05
t_3 increments	2390	1184	1184	2304
sw (t_3) (kHz)	100	59.524	59.524	100
Acq. Time (t_3) (ms)	11.95	9.94	9.94	11.52
^{1}H decoupling	SPINAL-64	SPINAL-64	SPINAL-64	SPINAL-64
Field (kHz)	90	80	72	90
Interscan delay (s)	2.9	2	1.9	3
Number of scans	32	40	48	16
Measurement time (h)	141	162	235	118

NMR data processing and analysis

2D and 3D spectra were processed using Bruker Biospin software Topspin 3.5, with a shifted squared cosine apodization function (SSB 2.2 to 3.0, depending on the spectra).
Solid-state NMR data were analysed with CcpNmr Analysis (Stevens et al., 2011; Vranken et al., 2005) and solution NMR data with CARA (Keller, 2004).

Assignment and data deposition

The amino-acid sequence used here corresponds to UniProtKB - P39990. Residue numbers corresponding to Snu13p solution NMR shifts, as deposited in the BioMagResBank under the accession number 15412, were corrected accordingly.

Assignment methodology

Partial backbone resonances assignment of Snu13p in the presence of Rsa1p[230-290] were obtained from ^{1}H-^{15}N HSQC, ^{1}H-^{13}C HSQC, HNCO, HN(CA)CO, HNCA, CBCANH and CBCA(CO)NH experiments and are listed in **ESM table 1**. An assigned ^{1}H-^{15}N HSQC is presented in the supplementary data (**ESM figure 2**). An intermediate exchange regime leading to broadened correlations doesn't allow for the acquisition of high quality 3D spectra, as stated in (Quinternet et al., 2016), thus preventing a complete resonance assignment.

In the ssNMR rotor, only one third of the SRH protein sample is labelled, namely roughly 6 mg of the 126-residue Snu13p. To acquire spectra with a signal to noise ratio comparable to the one obtained with a rotor completely filled with a protein of the same size, one would thus need 9 times longer. Considering this sensitivity issue, only a subset of the usual 2D and 3D assignment spectra (Habenstein et al., 2011; Schuetz et al., 2010) was recorded and is listed in **Table 1**, together with experimental details. The sequential walk is only possible through the carbonyl resonance C', thus not allowing for complete *de novo* assignments. Isolated ^{13}C signals show good typical linewidths of 0.5 ppm. Typical ^{15}N linewidths in indirect dimension are 1 ppm. 1D ^{13}C CP spectrum shows a S/N consistent with the amount and size of labelled protein in the rotor (data not shown).

ssNMR resonance assignment was therefore performed using solution NMR chemical shifts of free Snu13p (BMRB # 15412, sample in 50 mM Na-acetate, 50 mM NaCl, pH 5.5, measured at 293 K) and Snu13p in complex with Rsa1p[230-290]. Considering the experimental linewidths, ^{13}C assignments were transferred to the solid-state sample when observed correlations were isolated and within 0.5 ppm of the solution NMR-based predicted peak. Similarly, a threshold of 1 ppm was chosen for ^{15}N resonances. ssNMR assignments were then manually sequentially checked and extended using the whole set of recorded 2D and 3D spectra, as exemplified in **Figure 1**.

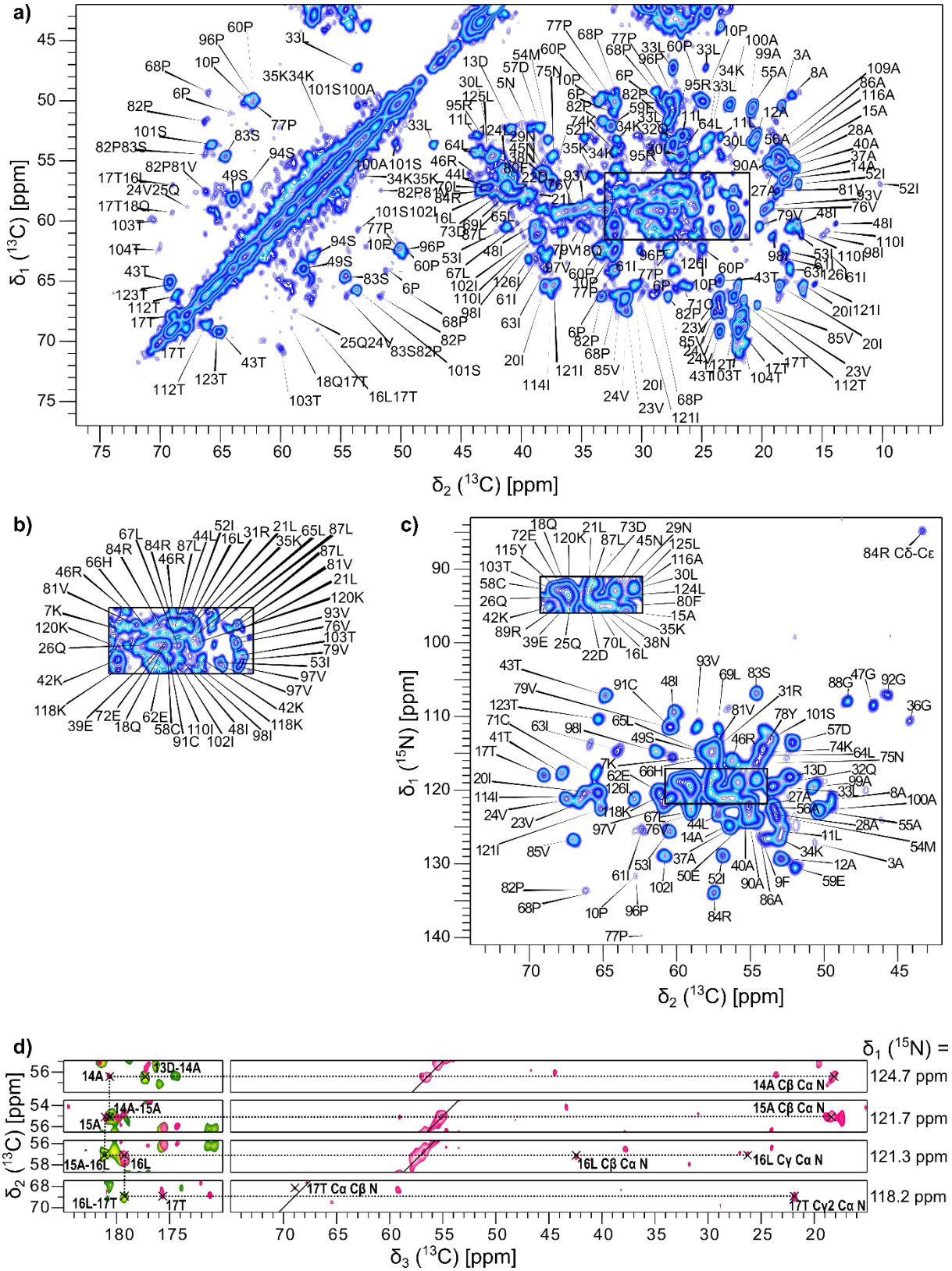

Figure 1: **a)** 2D ^{13}C-^{13}C extract of 50 ms DARR, showing intra-residue correlations, as well as some sequential contacts, labelled with the corresponding residue numbers and types. **b)** Assignments of the signals contained in the black rectangle of a). **c)** 2D ^{15}N-^{13}C NCA spectrum showing N-Cα intra-residue correlations labelled with residue type and number. Other correlation types (Arg Cδ-Cε) are indicated. The rectangle in the crowded region of the spectrum has been copied in the upper left for the sake of clarity. **d)** Sequential walk through carbonyl C' resonance for residues 14 to 17 from ^{13}C-^{13}C planes of NCACX and CANCO experiments, extracted at the indicated ^{15}N position.

Assignment statistics

91 out of 125 sequential contacts could be checked via 2D/3D experiments, facilitated by the existence of 82 unique amino-acid pairs in Snu13p sequence, leading to the assignment of 83% of the backbone, namely 81% N, 87% Cα and 81% C' resonances. 52% of side-chain non-H atoms were assigned, including 81% of Cβ. In total, assignment data could be obtained for 91% of the residues. Detailed assignment statistics are presented in **ESM table 2** and assigned spins are displayed in **Figure 2**.

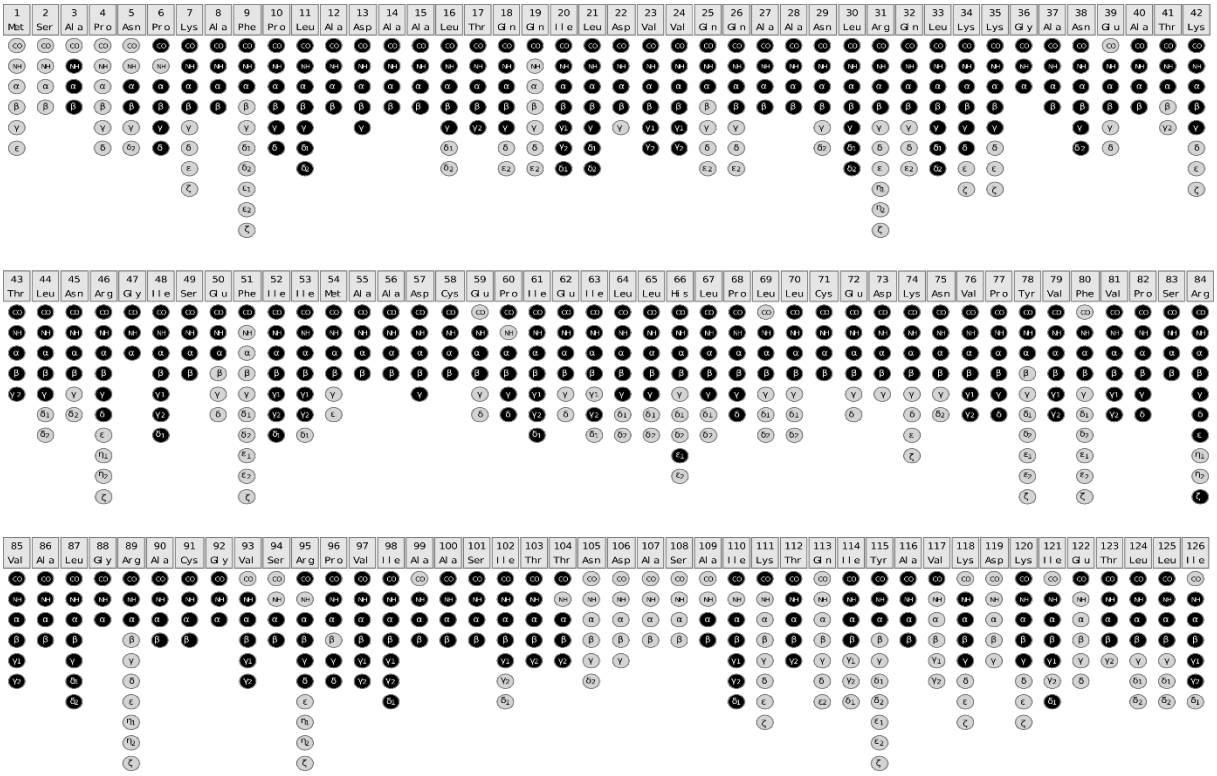

Figure 2: Assignment graph, created with CcpNmr software. Assigned spins are highlighted in black.

Solid-state NMR chemical shifts were deposited in the BioMagResBank (http://www.bmrb.wisc.edu) with the accession number 50110.

Secondary structure

Difference of $\Delta\delta(^{13}C\alpha)$ and $\Delta\delta(^{13}C\beta)$ secondary chemical shifts (SCS) is an indicator of the presence of α-helices and β-sheets. SCS are calculated by subtracting to the observed shifts the random coil shift from (Wang and Jardetzky, 2002). Three or more consecutive negative values indicate a β-sheet, four or more positive values are a hallmark of an α-helix (**Figure 3**).

As our solid-state NMR assignment is incomplete, TALOS-N (Shen and Bax, 2013) was also exploited for secondary structure analysis, as it also uses sequence-related data, which can be useful in protein regions lacking complete backbone assignments, in particular the last helix α5.

Snu13p ssNMR-derived secondary structure when bound to RH is presented in **Figure 3**. For comparison, free Snu13p solution NMR chemical shifts (BMRB #15412) were analysed with TALOS-N, as well. Secondary elements from X-ray data were obtained *via* DSSP (Kabsch and

Sander, 1983) for free Snu13p (PDB 2ALE) and Snu13p bound to Rsa1p[239-265] (PDB 4NUT).

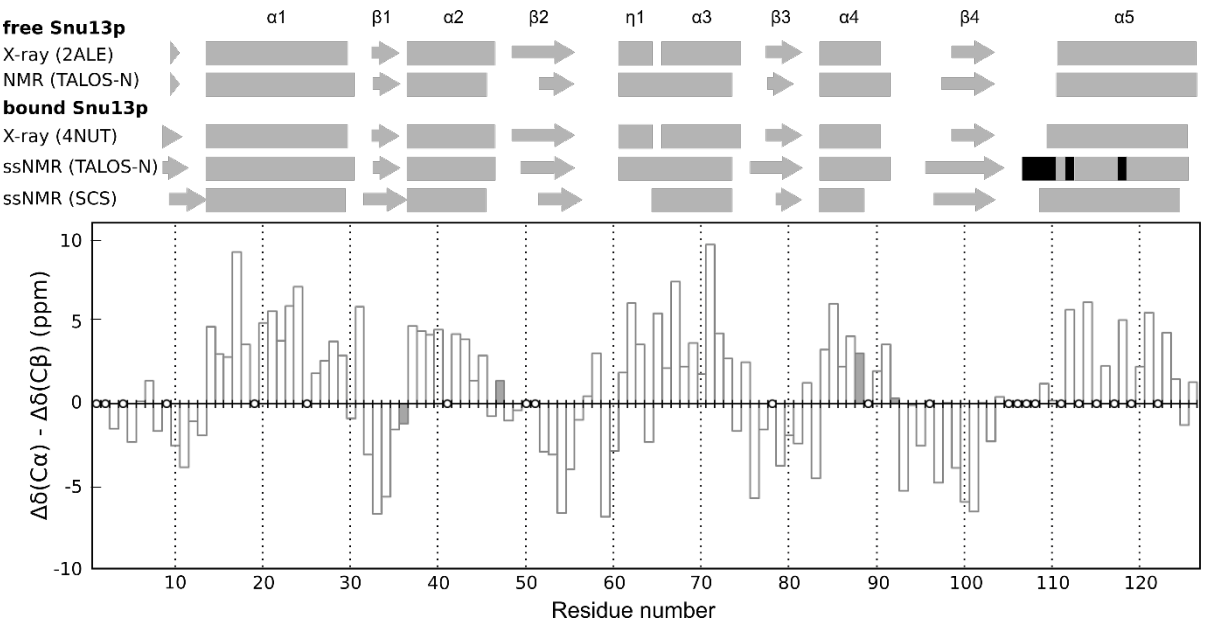

Figure 3: Snu13p secondary structure analysis. **Top:** free and bound Snu13p secondary structure elements derived from X-ray DSSP, solution NMR TALOS-N, ssNMR SCS and TALOS-N data. α-helices and β-sheets are drawn as rectangles and arrows, respectively. TALOS-N predictions based solely on the protein sequence are highlighted in black. **Bottom:** difference between Cα and Cβ secondary chemical shifts as a function of the residue number. Residues lacking Cα and/or Cβ assignment are displayed as empty circles. Glycine residues are plotted as dark grey bars, representing the difference between their Cα chemical shift and the random-coil value.

Observed differences in the exact boundaries of helices and strands between free and bound Snu13p may depend on the method used and are most probably influenced by the completeness of our ssNMR assignment. Differences between X-ray data of Snu13p or Snu13p[4-125]:Rsa1p[239-265] and ssNMR SRH data are mainly located in the last 30 residues of Snu13p (β4 strand and α5 helix), a region where nearly 30% of the backbone atoms assignment is missing, as well as in the first 10 residues, a domain which will be discussed in the following.
We compared X-ray 3D structures of Snu13p alone (PDB code 2ALE) and in complex with Rsa1p[239-265] (PDB code 4NUT) using SuperPose webserver (Maiti et al., 2004). They exhibit a main difference in the last helix α5. The backbone RMSD of 1.36 Å goes down to 0.59 Å when not considering the last 20 residues.

In poorly assigned β4-α5 loop, T103 and T104 Cα-Cβ DARR correlation peaks are small and broad, possibly multiple, pointing to different coexisting conformations at the experiment's timescale.

Snu13p overall secondary structure is maintained in the context of our SRH complex, when compared to free Snu13p. Moreover, there is no major difference in the secondary structure elements when Snu13p is bound solely to Rsa1p[239-265] or – like in our ssNMR sample – to RH, a result supporting the hypothesis in (Quinternet et al., 2016) of independent Snu13p:Rsa1p and Rsa1p:Hit1p modules in the tripartite Snu13p:Rsa1p:Hit1p complex.

Free Snu13p in solution *vs.* Snu13p in the SRH complex: chemical shift perturbations (CSPs)

We exploited chemical shift perturbations (CSPs) to gain a better insight on Snu13p structural changes occurring upon RH binding.

CSPs are calculated according to (Williamson, 2013) as the Euclidean distance between Snu13p ssNMR chemical shifts in the SRH complex and chemical shifts of free Snu13p in solution (Workman et al., 2008).

Calculated {Cα, Cβ} CSPs are plotted in **Figure 4a** and considered significant when they are at least larger than the standard deviation.

Absolute differences in Cα and Cβ chemical shifts when comparing Snu13p in SRH with free Snu13p have a mean value of 0.5 and 0.4 ppm, respectively. These values drop to 0.1 and 0.2 ppm when comparing ssNMR SRH chemical shifts to the ones of Snu13p bound to Rsa1p[230-290] (**ESM table 1**), confirming that in some extent, our ssNMR CSP data account for a real effect of RH binding.

As stated above, Snu13p X-ray structures point to a change in α5 helix position upon binding of Rsa1p[239-265], which in turn could be responsible for numerous conformational changes leading to large CSPs far from the Snu13p:Rsa1p interface, thus hampering a clear identification of the residues involved in the interaction. In addition, the presence of a C-terminal extension solely in free Snu13p constructs, used both for X-ray and solution NMR studies, might also contribute, to some extent, to additional chemical shift changes. Indeed, the observed CSPs in α5 helix belong to the larger ones.

As a possible consequence of α5 helix rigid-body motion, regions in Snu13p hydrophobic core show significant {Cα, Cβ} CSPs, pointing to indirect local conformational changes upon complex formation. They involve one side of α1 helix (T17, I20, L21, V24, A27, A28), A12 in the loop preceding α1 and pointing to the same side, and residues facing this helix's side, namely K35 in β1 strand, I52 and I53 in β2 strand, V79 in β3 strand, S101 and I102 in β4 strand. L67 and K74, both located on the same side of α5 helix and also facing affected residues in these strands, show significant CSPs as well. A 3D structure highlighting these regions is presented in **ESM figure 3**.

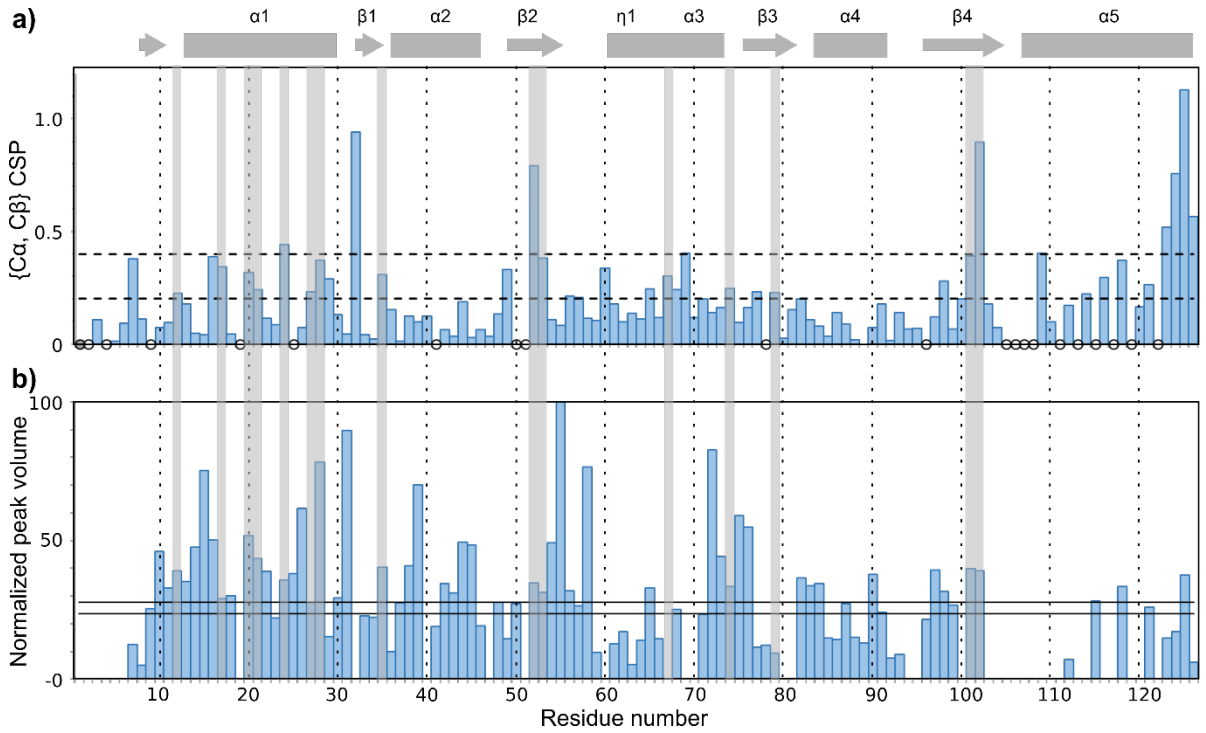

Figure 4: **a)** {Cα,Cβ} CSPs as a function of the residue number, to compare free Snu13p with Snu13p in the SRH complex. Dotted lines represent one and two times the standard deviation. Unassigned residues in Snu13p solution and in SRH are represented as filled and empty circles, respectively. Snu13p predicted helices and strands in SRH complex, as derived from ssNMR data via TALOS-N, are plotted on top as rectangles and arrows, respectively. **b)** Normalized peak volumes from 3D CANCO experiment plotted as a function of residue number i for $C\alpha_i$-N_i-$C'_{(i-1)}$ correlations. Solid lines are drawn at the mean volume +/- standard deviation. Regions in the hydrophobic core of Snu13p experiencing significant CSPs are highlighted with light grey rectangles.

With a view to further filtering out possible irrelevant data, we analysed CSPs in combination with dynamics data derived from 3D CANCO peak volumes, as displayed in **Figure 4b**.
3D CANCO peak volumes are indeed related to the efficiency of ^{15}N-^{13}C transfers, largely influenced by dipolar couplings. Thus, in a first approximation, smaller peaks can be linked to more mobile residues, bigger peaks to more rigid regions.

Although α5 helix is the domain lacking the most assigned residues, A116, K118, T123, L124 and L125 show significant {Cα, Cβ} CSPs. CANCO peak volumes point to a rather mobile region where K118 and L125 seem to be outlier rigid residues located on the same side of α5. C-terminal residues being generally mobile, K118 and L125 are part of the interaction interface, as observed on sub-complex structure (PDB 4NUT) with respectively I257 and N259, and W253, K250, L254 of Rsa1p. On this same helix's side, E122 interacts with Rsa1p H264 (Quinternet et al., 2016). Unfortunately, only C' E122 resonance was assigned in ssNMR SRH: its chemical shift difference to free Snu13p E122 C' resonance is 2.8 ppm, which is quite large and significant.

Amongst Snu13p in N-terminal residues preceding α1 helix, K7 has a CSP larger than the standard deviation and could be affected by Rsa1p N-terminal residues proximity, notably *via* an interaction with Rsa1p V242, not described in previous structural studies. In Snu13p N-terminal domain, our incomplete ssNMR data regarding F9 show a N shift of 5.3 ppm when compared to the free Snu13p case. It is in agreement with our observation, on the sub-complex X-ray structure (PDB 4NUT), of a proximity between F9 and Rsa1p residue R246, but also between F9 and L125 sidechains. Globally, these new inter- and intra-

molecular contacts, displayed in **ESM figure 3**, might help bringing Snu13p N-terminal and C-terminal residues close to Rsa1p, leading to the above-mentioned CSPs and the rigidity of pre-α1 loop and C-terminal extremity of α5 helix.

The overall low volume of CANCO assigned peaks from residues 61 to 71 (η1 helix and beginning of α3 helix) points to a rather mobile region of the protein. In this stretch, L65 is rigid. There is unfortunately no L69 correlation peak in 3D CANCO to check this hypothesis, but L65 and L69 both show significant {Cα, Cβ} CSPs and were previously reported as essential in Snu13p hydrophobic interaction with Rsa1p (Bizarro et al., 2014; Rothé et al., 2014a).

Previous studies have also identified E72 as a critical residue for Rsa1p binding through electrostatic interaction (Bizarro et al., 2014; Rothé et al., 2014a). Our ssNMR results show however no significant {Cα, Cβ} CSP, but a 3.2 ppm difference in C' chemical shift. E72 belongs to a rather rigid stretch spanning residues 72 to 76. Additional differences with respect to free Snu13p might have been observed by comparing E72 side-chains assignments, which could unfortunately not be obtained in our ssNMR SRH sample.

Snu13p interaction with Rsa1p:Hit1p must be labile to achieve its biological function because these assembly factors are not found in the final mature particle. We recorded first ssNMR spectra of the same SRH complex, where Snu13p is unlabelled and RH is fully ^{13}C and ^{15}N enriched. Intensity of 1D CP ^{13}C spectra is lower than expected, when compared to SRH with labelled Snu13p and taking into account the amount of labelled protein in the rotor (data not shown). Moreover, a ssNMR 2D proton-detected ^{15}N-^{1}H experiment with INEPT transfers (**ESM figure 4**) shows the presence of roughly 60 highly mobile residues, probably comprising Rsa1p linker region [260-316]. Rsa1p:Hit1p internal dynamics and possible conformational heterogeneity could be responsible for the difficulty of assigning some Snu13p residues and identifying a clearer interaction interface by simple CSP analysis.

Conclusion

Snu13p ssNMR assignments in the context of the 50 kDa SRH complex show that Snu13p overall secondary structure is maintained upon RH binding.
Even if CSP analysis is hampered by the lack of assignment data in some regions, we were able to confirm most of the interaction sites of Snu13p identified in studies involving sub-complexes and shorter Rsa1p constructs than the one used in our SRH ssNMR sample. We also evidenced additional involvement of Snu13p N-terminal and C-terminal residues: upon RH binding, hydrophobic contacts between F9 and L125 bring the extremities of Snu13p together, and seem to promote a contact between Snu13p N-terminal residues and Rsa1p like F9 with R246, K7 with V242.

ssNMR Snu13p assigned resonances when bound to RH will serve as a basis for future interaction studies to decipher the snoRNP assembly pathway.
In particular, it will be interesting to add RNA to the SRH complex to gain a better understanding of RNA binding and possible protein rearrangements. RNAse protection experiments have shown a direct interaction between Rsa1p and the 5' domain of snoRNA U3 (Rothé et al., 2017).The U3 snoRNA fragment including the two boxes B/C and C'/D and

the 5' domain represents a good candidate. From the titration NMR experiments of Snu13p by box C/D U14 snoRNA recently published (Chagot et al., 2019), we identified the key residues in interaction with RNA: E39, E59, I63, R84 from VPSR motif, and I98. For these key residues, ssNMR assignments of Snu13p in the SRH complex are available.

References

Bachellerie, J.-P., Cavaillé, J., Hüttenhofer, A. (2002) The expanding snoRNA world. Biochimie 84:775–790. https://doi.org/10.1016/S0300-9084(02)01402-5

Bizarro, J., Charron, C., Boulon, S., Westman, B., Pradet-Balade, B., Vandermoere, F., Chagot, M.-E., Hallais, M., Ahmad, Y., Leonhardt, H., Lamond, A., Manival, X., Branlant, C., Charpentier, B., Verheggen, C., Bertrand, E. (2014) Proteomic and 3D structure analyses highlight the C/D box snoRNP assembly mechanism and its control. J Cell Biol 207:463–480. https://doi.org/10.1083/jcb.201404160

Böckmann, A., Gardiennet, C., Verel, R., Hunkeler, A., Loquet, A., Pintacuda, G., Emsley, L., Meier, B.H., Lesage, A. (2009) Characterization of different water pools in solid-state NMR protein samples. J Biomol NMR 45:319–327. https://doi.org/10.1007/s10858-009-9374-3

Boulon, S., Marmier-Gourrier, N., Pradet-Balade, B., Wurth, L., Verheggen, C., Jády, B.E., Rothé, B., Pescia, C., Robert, M.-C., Kiss, T., Bardoni, B., Krol, A., Branlant, C., Allmang, C., Bertrand, E., Charpentier, B. (2008) The Hsp90 chaperone controls the biogenesis of L7Ae RNPs through conserved machinery. J Cell Biol 180:579–595. https://doi.org/10.1083/jcb.200708110

Chagot, M.-E., Quinternet, M., Rothé, B., Charpentier, B., Coutant, J., Manival, X., Lebars, I. (2019) The yeast C/D box snoRNA U14 adopts a “weak” K-turn like conformation recognized by the Snu13 core protein in solution. Biochimie 164:70–82. https://doi.org/10.1016/j.biochi.2019.03.014

Dobbyn, H.C., McEwan, P.A., Krause, A., Novak-Frazer, L., Bella, J., O’Keefe, R.T. (2007) Analysis of pre-mRNA and pre-rRNA processing factor Snu13p structure and mutants. Biochem Biophys Res Commun 360:857–862. https://doi.org/10.1016/j.bbrc.2007.06.163

Habenstein, B., Wasmer, C., Bousset, L., Sourigues, Y., Schütz, A., Loquet, A., Meier, B.H., Melki, R., Böckmann, A. (2011) Extensive de novo solid-state NMR assignments of the 33 kDa C-terminal domain of the Ure2 prion. Journal of Biomolecular NMR 51:235–243. https://doi.org/10.1007/s10858-011-9530-4

Kabsch, W., Sander, C. (1983) Dictionary of protein secondary structure: Pattern recognition of hydrogen-bonded and geometrical features. Biopolymers 22:2577–2637. https://doi.org/10.1002/bip.360221211

Keller, R. (2004) The computer aided resonance assignment tutorial. Cantina Verl., Goldau.

Lafontaine, D.L.J. (2015) Noncoding RNAs in eukaryotic ribosome biogenesis and function. Nat Struct Mol Biol 22:11–19. https://doi.org/10.1038/nsmb.2939

Maiti, R., Van Domselaar, G.H., Zhang, H., Wishart, D.S. (2004) SuperPose: a simple server for sophisticated structural superposition. Nucleic Acids Research 32:W590–W594. https://doi.org/10.1093/nar/gkh477

Paul, A., Tiotiu, D., Bragantini, B., Marty, H., Charpentier, B., Massenet, S., Labialle, S. (2019) Bcd1p controls RNA loading of the core protein Nop58 during C/D box snoRNP biogenesis. RNA 25:496–506. https://doi.org/10.1261/rna.067967.118

Peng, Y., Yu, G., Tian, S., Li, H. (2014) Co-Expression and Co-Purification of Archaeal and Eukaryal Box C/D RNPs. PLoS ONE 9:e103096. https://doi.org/10.1371/journal.pone.0103096

Quinternet, M., Chagot, M.-E., Rothé, B., Tiotiu, D., Charpentier, B., Manival, X. (2016) Structural Features of the Box C/D snoRNP Pre-assembly Process Are Conserved through Species. Structure 24:1693–1706. https://doi.org/10.1016/j.str.2016.07.016

Rothé, B., Back, R., Quinternet, M., Bizarro, J., Robert, M.-C., Blaud, M., Romier, C., Manival, X., Charpentier, B., Bertrand, E., Branlant, C. (2014a) Characterization of the interaction between protein Snu13p/15.5K and the Rsa1p/NUFIP factor and demonstration of its functional importance for snoRNP assembly. Nucleic Acids Research 42:2015–2036. https://doi.org/10.1093/nar/gkt1091

Rothé, B., Manival, X., Rolland, N., Charron, C., Senty-Ségault, V., Branlant, C., Charpentier, B. (2017) Implication of the box C/D snoRNP assembly factor Rsa1p in U3 snoRNP assembly. Nucleic Acids Research 45:7455–7473. https://doi.org/10.1093/nar/gkx424

Rothé, B., Saliou, J.-M., Quinternet, M., Back, R., Tiotiu, D., Jacquemin, C., Loegler, C., Schlotter, F., Peña, V., Eckert, K., Morera, S., Dorsselaer, A.V., Branlant, C., Massenet, S., Sanglier-Cianférani, S., Manival, X., Charpentier, B. (2014b) Protein Hit1, a novel box C/D snoRNP assembly factor, controls cellular

concentration of the scaffolding protein Rsa1 by direct interaction. Nucleic Acids Res 42:10731–10747. https://doi.org/10.1093/nar/gku612

Schuetz, A., Wasmer, C., Habenstein, B., Verel, R., Greenwald, J., Riek, R., Böckmann, A., Meier, B.H. (2010) Protocols for the Sequential Solid-State NMR Spectroscopic Assignment of a Uniformly Labeled 25 kDa Protein: HET-s(1-227). ChemBioChem 11:1543–1551. https://doi.org/10.1002/cbic.201000124

Schultz, A., Nottrott, S., Watkins, N.J., Luhrmann, R. (2006) Protein-Protein and Protein-RNA Contacts both Contribute to the 15.5K-Mediated Assembly of the U4/U6 snRNP and the Box C/D snoRNPs. Molecular and Cellular Biology 26:5146–5154. https://doi.org/10.1128/MCB.02374-05

Shen, Y., Bax, A. (2013) Protein backbone and sidechain torsion angles predicted from NMR chemical shifts using artificial neural networks. J Biomol NMR 56:227–241. https://doi.org/10.1007/s10858-013-9741-y

Stevens, T.J., Fogh, R.H., Boucher, W., Higman, V.A., Eisenmenger, F., Bardiaux, B., van Rossum, B.-J., Oschkinat, H., Laue, E.D. (2011) A software framework for analysing solid-state MAS NMR data. Journal of Biomolecular NMR 51:437–447. https://doi.org/10.1007/s10858-011-9569-2

Vranken, W.F., Boucher, W., Stevens, T.J., Fogh, R.H., Pajon, A., Llinas, M., Ulrich, E.L., Markley, J.L., Ionides, J., Laue, E.D. (2005) The CCPN data model for NMR spectroscopy: Development of a software pipeline. Proteins: Structure, Function, and Bioinformatics 59:687–696. https://doi.org/10.1002/prot.20449

Wang, Y.J., Jardetzky, O. (2002) Probability-based protein secondary structure identification using combined NMR chemical-shift data. Protein Sci 11:852–861.

Watkins, N.J., Dickmanns, A., Luhrmann, R. (2002) Conserved Stem II of the Box C/D Motif Is Essential for Nucleolar Localization and Is Required, Along with the 15.5K Protein, for the Hierarchical Assembly of the Box C/D snoRNP. Molecular and Cellular Biology 22:8342–8352. https://doi.org/10.1128/MCB.22.23.8342-8352.2002

Williamson, M.P. (2013) Using chemical shift perturbation to characterise ligand binding. Progress in Nuclear Magnetic Resonance Spectroscopy 73:1–16. https://doi.org/10.1016/j.pnmrs.2013.02.001

Workman, H., Skalicky, J.J., Flynn, P.F. (2008) Assignment of 1H, 13C, and 15N resonances of the RNA binding protein Snu13p from Saccharomyces cerevisiae. Biomolecular NMR Assignments 2:1–3. https://doi.org/10.1007/s12104-007-9069-1